Inorganic Chemistry

ARTICLE

pubs.acs.org/IC

Experimental Charge Density Analysis of a Gallium(I) N-Heterocyclic Carbene Analogue

Jacob Overgaard,*[,†,‡] Cameron Jones,[‡] Deepak Dange,[‡] and James A. Platts[§]

[†]Department of Chemistry & Centre for Materials Crystallography, Aarhus University, Langelandsgade 140, DK-8000 Aarhus C, Denmark

[‡]School of Chemistry, P.O. Box 23, Monash University, Melbourne, VIC, 3800, Australia

[§]School of Chemistry, Cardiff University, Park Place, Cardiff CF10 3AT, U.K.

Supporting Information

ABSTRACT: The experimental electron density of the only known example of a four-membered Ga(I) N-heterocyclic carbene analogue has been determined by multipole modeling of 90 K X-ray diffraction data and compared to theoretical data. In order to obtain a satisfactory model, it is necessary to modify the radial dependency of the core electrons of Ga using two separate scaling parameters for s,p- and d-electrons. Evidence for significant lone-pair density on Ga is found in the electron density and derived properties despite the partial positive charge of this atom. Static deformation density and molecular electrostatic potential clearly show a directional lone pair on Ga, whereas the Laplacian of the total electron density does not; this feature is, however, present in the Laplacian of the valence-only density. The Ga center also acts as an acceptor in four intramolecular C−H···Ga contacts, whose nature is probed by density properties. Substantial covalent character is apparent in the Ga−N bonds, but no sign of donation from filled N p-orbitals to empty Ga p-orbitals is found, whereas π-delocalization over the organic ligand is evident. This study highlights the utility of experimental charge density analysis as a technique to investigate the unusual bonding and electronic characteristics of low oxidation state/low coordinate p-block complexes.

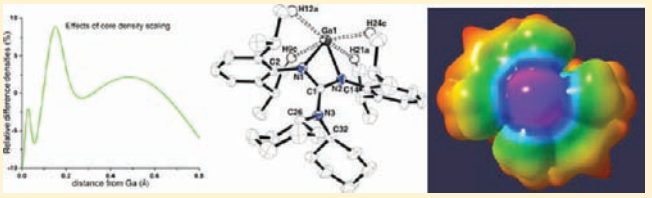

INTRODUCTION

The low oxidation state chemistry of the heavier main group elements has rapidly expanded over the past two decades.[1] This has given rise to numerous fascinating complex types, which, in many cases, exhibit unusual structural and bonding patterns, the nature of which is often hotly debated in the literature.[2] In order to gain an understanding of these patterns, a variety of theoretical techniques have been applied to the analysis of bonding in low oxidation state systems. However, the interpretation of the results from such analyses often leads to contradictory conclusions, even when spectroscopic data are available for the compounds in question.[1−3] Accordingly, it would be of great benefit to apply nonspectroscopic experimental techniques to the analysis of the bonding and electronic properties of low oxidation state main group complexes and to compare the results of these analyses with those from theoretical studies. Experimental charge density studies, derived from high quality X-ray crystallographic data, provide the opportunity to achieve this. One particular advantage of the experimental charge density method is that it provides an analytical description of the electron density, which can be analyzed according to the quantum theory of atoms in molecules (QTAIM),[4] thus providing quantitative information about the interatomic bonding, which may be compared to an identical approach to theoretical data. Successful application of this method requires accurate intensity data and is becoming increasingly widespread due to the enhanced performance of diffractometer technology, such that this approach has been applied to solve numerous chemical questions.[5]

There have been a few reports of the electron density distribution in compounds containing low-valent main group elements, one of these being a study of a Si(II) monohydride.[6] In two other recent studies,[7] it has been shown that valuable information on the highly unusual metal−metal bonding in a magnesium(I) dimer, $[\{(DipNCMe)_2CH\}Mg]_2$ (Dip = 2,6-diisopropylphenyl), can indeed be gained from experimental charge density studies, in this case showing a non-nuclear attractor between the two metal atoms. With the aim of applying this technique for the first time to low oxidation state heavier group 13 metal complexes, we have investigated the four-membered gallium(I) heterocycle, [:Ga(I)Giso)] **1** (Giso = $[(DipN)_2CN(C_6H_{11})_2]^-$.[8] This compound is kinetically stabilized by the incorporation of a very bulky guanidinate ligand[9] and exhibits a two-coordinate gallium center, formally in the +1 oxidation state and bearing a lone pair of electrons. In view of this, compound **1** falls into the class of heavier p-block N-heterocyclic carbene (NHC) analogues, the coordination and other chemistry of which is rapidly emerging.[10] A theoretical study

Received: May 11, 2011
Published: August 02, 2011

carried out on a model of **1** indicated that while its Ga lone pair possesses a high degree of s-character ($4s^{1.90}4p^{0.37}$ by natural bond orbital, NBO, analysis), it exhibits sufficient directionality for the heterocycle to behave as an unconventional gallium σ-donor ligand toward transition metal fragments. In contrast, the high energy of its lowest unoccupied molecular orbital (consisting largely of an empty p-orbital at Ga) implied that the heterocycle would be a weak π-acceptor ligand.[8] Subsequent synthetic studies confirmed both hypotheses.[11]

Here, we describe the results of an experimental charge density study on **1**, which, in combination with theoretical analysis, not only validates the presence of a weakly directional lone pair of electrons at its Ga center but also allows for an in-depth picture of its electronic structure to be assembled. To the best of our knowledge, only one previous study has employed such methods to study the electron density in a low-valent group 13 complex: Flierler et al. examined the density in a dinuclear "borylene" complex, concluding that this should be classified as a dimetalloborane rather than a borylene.[12] In contrast, our use of a very bulky guanidinate ligand allows the isolation and study of the gallylene itself, free from the effects of metal complexation. Moreover, as first pointed out by Bader[13] and recently studied in great detail in a series of papers by Scherer et al.,[14,15] the electron density due to the shell structure of elements heavier than argon is more complex than for lighter elements such as boron. In particular, the valence n quantum shell is not observed in the Laplacian of the electron density, and instead the outer core $(n-1)$ shell is polarized by the presence of ligands, giving rise to ligand-induced charge concentrations (LICCs) in these formally core orbitals. Such analysis has, to date, only been applied to s- and d-block elements such as Ca, Ti, and Nb: the current study is the first attempt to analyze these effects in a heavy p-block element. The main analysis will focus on a description of the spatial location of Ga lone pair density, which finds no precedent in the charge density literature.

EXPERIMENTAL AND COMPUTATIONAL METHODS

A single crystal specimen of **1** was selected and mounted in the cold stream (90 K) from an Oxford Cryosystems cooling device, and it was allowed to thermally equilibrate for 15 min before data collection was carried out using a Mo X-ray source from an Oxford Diffraction Excalibur diffractometer. A total of 220 446 measured intensities were integrated with the CrysAlis software,[16] and a face-indexed absorption correction was performed using the ABSPACK program.[17] The data were merged with SORTAV,[18] resulting in the removal of 704 severe outliers to yield 35 419 unique reflections to a maximum resolution of 1.08 $Å^{-1}$ and a completeness of 98.8%. The internal agreement was 2.80%. The unit cell parameters refined to a = 9.6399(2) Å, b = 10.5617(1) Å, c = 17.7407(2) Å, α = 107.1032(12)°, β = 95.2802(12)°, and γ = 97.5155(12)°. The crystal structure was solved in space group $P1$ by direct methods.[19] The final independent atom model (IAM) consisted of 378 parameters and converged to give $R(F)$ = 3.8%, goodness-of-fit = 0.73 for all 35 419 reflections. This model served as a starting point for the multipole modeling (using the atom-centered Hansen−Coppens formalism[20]) of the charge density using the program XD.[21]

It is well documented that the description of the hydrogen atomic parameters including anisotropic displacement is crucial in the search for a satisfactory charge density model.[22] Our approach to the refinement was thus chosen in accordance with both our own experience[23] and some recommendations given recently.[24] Therefore, an initial high-order refinement ($\sin(\theta)/\lambda > 0.8$ $Å^{-1}$) was employed to fix the positions and atomic displacement parameters (ADPs) for all non-hydrogen atoms, followed by refinement of hydrogen atom positions and isotropic ADPs using all 9443 data below 0.7 $Å^{-1}$, with X−H bond distances fixed to standard values from neutron diffraction.[25] From this model, anisotropic thermal parameters were calculated using the SHADE2 web utility.[26] All atomic position and thermal motion parameters were then fixed at these values, and multipole modeling of electron density was attempted. $R(F^2)$ values decreased as 4.14%, 3.84%, 2.74%, and 2.62% when l_{max} was increased incrementally from 1 to 4. The details of the exact procedures for multipole modeling are expanded in the following paragraphs, while a detailed account of the procedure can be found in the Supporting Information. Important crystallographic information is listed in Table 1. This multipole model of experimental diffraction data is denoted model **A**, and an ORTEP drawing based on this is shown in Figure 1.

Table 1. Crystallographic Details

	A	B
formula	$Ga_1C_{37}H_{56}N_3$	
formula weight, g mol^{-1}	612.57	
crystal size, mm	0.39 × 0.25 × 0.20	
crystal system, space group	triclinic, $P\bar{1}$	triclinic, $P1$
λ, Å	0.71073	
T, K	90(1)	0
a, Å	9.6399(2)	20
b, Å	10.5617(1)	20
c, Å	17.7407(2)	20
α, °	107.1032(12)	90
β, °	95.2802(12)	90
γ, °	97.5155(12)	90
V, $Å^3$	1695.23(4)	
$F(000)$	660	
μ, mm^{-1}	0.84	
T_{max}, T_{min}	0.881, 0.776	
$\sin(\theta)/\lambda_{max}$, Å	1.08	1.10
N_{meas}, N_{unique}	220446, 35419	133874
R_{int}	0.028	
average redundancy	6.2	
completeness	0.988	
N_{obs}, N_{var}; $(F^2 > 2\sigma(F^2))$	29483, 753	133874, 1056
$R(F)$, $R(F^2)$; $F^2 > 2\sigma(F^2)$	0.0191, 0.0194	
$R(F)$, $R(F^2)$; all data	0.0347, 0.0211	0.0017, -
goodness-of-fit	0.898	

Cartesian coordinates of a single molecule of **1** were extracted from the final refinement and used in theoretical studies without further modification. All theoretical data were obtained at the density functional theory (DFT) BP86/6-31+G(d,p) level[27] using Gaussian03.[28] Satisfactory convergence required use of density fitting, previously shown to have no noticeable effect on calculated electron density data.[7b] Electron density properties from theoretical data were evaluated using the AIMPAC, AIM2000, and AIMAll packages,[29] while further data on atomic and orbital populations were obtained from the natural bond orbital (NBO) method.[30] An isolated molecule of **1** was placed in a cubic unit cell measuring 20 Å in length and used to generate theoretical structure factors to a $(\sin\theta/\lambda)$ limit of 1.1 $Å^{-1}$ using DENPROP.[31] The resulting projected density described in terms of a multipole model is denoted model **B**, whereas the primary density taken directly from DFT will be denoted model **C**. Full details of model **B** are reported in Supporting Information.

RESULTS AND DISCUSSION

Initially, the scattering factor for Ga was that for the neutral atom taken from the internal data bank of XD, with $[Ar]3d^{10}$ core

dx.doi.org/10.1021/ic2009946 |Inorg. Chem. 2011, 50, 8418–8426

and $4s^2 4p^1$ electrons in the valence shell, because the monovalent Ga^+ scattering factor is not available in the data bank.[32] Using this scattering factor in the IAM refinement resulted in a large peak of unmodeled residual density (0.9 e Å^{-3}) close to the Ga-position (Figure 2a), which was barely affected by the introduction of multipoles or different combinations of (n,ξ_l) in the description of the radial functions for valence density. The residual density on Ga could not be removed by the introduction of anharmonic thermal parameters, in contrast to what a recent study by Pinkerton et al. suggested.[33] Multipole modeling using theoretical structure factors **B** showed the same problem (residual density on Ga of 0.3 e Å^{-3}), and it was found that this residual density could be significantly reduced by scaling the radial dependencies of the Ga core densities for the 10 d-, 18 s-, and p-electrons using the κ-parameters available in the multipole model; this dramatically improved the fit, as shown in Figure 2b. Core scaling parameters (κ) derived from theoretical data **B** were 0.9577(1) for the s,p-electrons and 1.0591(1) for the d-electrons, i.e., the s,p-electrons are expanded and the d-electrons are contracted, both sets by ca. 5% relative to the neutral atom in the gas-phase. The absolute changes observed in the radial dependency compared to the neutral atom are significantly larger here than previously observed in an experimental charge density study of Corundum.[34]

Our expectation was that convergence in the refinement of this type of core scaling against experimental diffraction data would be difficult to achieve, but we found that both core-scaling parameters could be refined, leading to very similar values to those found from theoretical data (κ-parameters of 0.964(1) and 1.046(2) for s,p-electrons and d-electrons, respectively). In contrast, a single core scaling parameter, as used in our recent study of subvalent Mg[1,7] did not satisfactorily reduce the residual density. The final model was therefore made using experimentally refined core scaling parameters, such that the final model of experimental data (**A**) does not rely on model **B** in any way. The latter model is not subject to experimental noise nor to effects such as absorption or extinction that might complicate matters. However, it is based on a representation of the electron density in a Gaussian basis set, which does not have the correct shape at nuclear positions. Nevertheless, the fact that essentially identical adjustments of the tabulated Ga core density appear from independent experimental and theoretical approaches lends credence to the physical significance of this effect. Full examination of the origin and generality of such features is beyond the scope of this paper and will be treated in more detail in a subsequent publication.

Following the refinements of this Ga split-core model, the inclusion of hexadecapoles on C atoms was found to be significant, leading to a substantial improvement of fit and reduction in $R(F^2)$ from 2.07% to 1.94%. The residual density map based on this final model (**A**) is shown in Figure 2b.

With a satisfactory model of the electron density in **1**, properties of the valence density can be examined in detail. Table 2 reports the topological properties of selected bond and ring critical points from models **A** and **C**. Agreement between experiment and theory is good, with all important features reproduced by both methods. Ga−N bonds exhibit low values of electron density (ρ) and small, positive values of $\nabla^2\rho$ at the bond critical point (bcp), and the contrast between these and the more typically covalent N−C bond is clear. However, energy density data indicate that potential energy dominates even in the Ga−N bonds, such that they are predicted to have significant covalent character. Parameters such as kinetic energy per electron ($G(r)$) and ratio of potential to kinetic energy also indicate covalent character in the Ga−N bonds. The ellipticity in the Ga−N bonds is rather low, which suggests that these are σ-type bonds, with no π-interaction between the formally filled N p-orbitals and empty Ga p-orbitals orthogonal to the heterocycle plane, supporting the proposed poor π-acceptor ability of Ga. It is unlikely that the difference in ε between Ga−N(1) and Ga−N(2) is significant, as all other properties of these bonds are

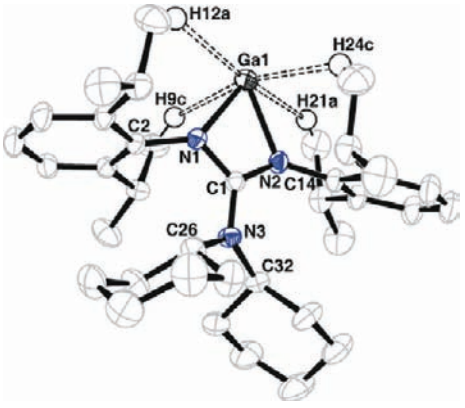

Figure 1. ORTEP drawing of **1** shown at 90% probability ellipsoids. The hydrogen atoms are omitted for clarity, except for the four H atoms involved in intramolecular contacts with Ga.

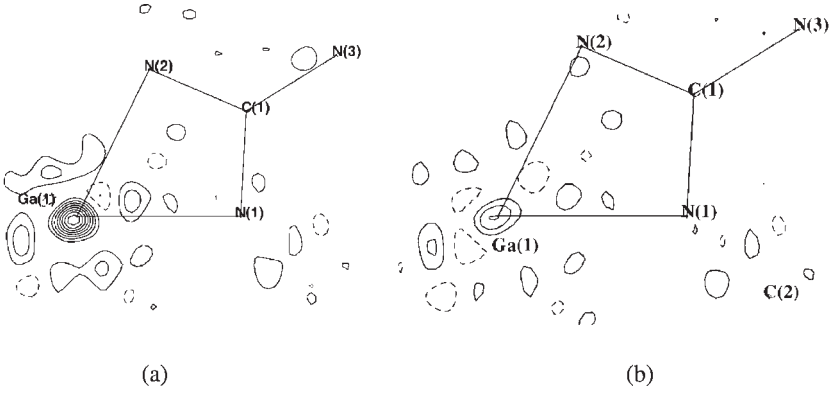

Figure 2. Residual density maps for **A** in the Ga−N−C−N plane, with contours at 0.1 e Å^{-3}: (a) based on a single core scale factor for Ga and (b) based on separate scaling of s,p- and d-core electrons for Ga.

dx.doi.org/10.1021/ic2009946 |*Inorg. Chem.* 2011, 50, 8418–8426

Table 2. Topological Properties at Selected Critical Points from Models A and C[a]

bond	ρ (e Å^{-3})	$\nabla^2\rho$ (e Å^{-5})	d(1-2) (Å)	d(1-bcp) (Å)	d(2-bcp) (Å)	ε	G (hartree Å^{-3})	V (hartree Å^{-3})	H (hartree Å^{-3})	G/ρ (hartree e^{-1})
Ga(1)−N(1)	0.56(1)	5.44(2)	2.091	1.05	1.05	0.10	0.56	−0.74	−0.18	1.00
	0.50	5.27		0.99	1.10	0.06	0.51	−0.65	−0.14	1.02
Ga(1)−N(2)	0.56(1)	5.39(2)	2.094	1.05	1.05	0.03	0.56	−0.74	−0.18	1.00
	0.49	5.20		0.99	1.10	0.06	0.50	−0.64	−0.14	1.01
N(1)−C(1)	2.40(2)	−26.49(8)	1.350	0.78	0.57	0.15	1.41	−4.71	−3.30	0.62
	2.27	−27.09		0.83	0.52	0.20	1.41	−4.72	−3.31	0.62
N(2)−C(1)	2.41(2)	−24.95(8)	1.351	0.77	0.58	0.15	1.41	−4.71	−3.30	0.62
	2.27	−27.01		0.83	0.52	0.20	1.41	−4.72	−3.31	0.62
N(3)−C(1)	2.30(2)	−24.48(8)	1.373	0.80	0.58	0.19	1.31	−4.34	−3.03	0.61
	2.14	−24.59		0.85	0.52	0.22	1.35	−4.42	−3.07	0.63
Ga−NCN ring	0.33(1)	4.84(1)					0.35	−0.37	−0.01	1.07
	0.29	4.67					0.32	−0.31	+0.01	1.10
					Ga···H Interactions					
Ga(1)−H(9C)	0.049(3)	0.684(1)	2.586	1.00	1.59	0.39	0.04	−0.03	0.01	0.76
	0.078	0.598		1.04	1.55	0.22	0.04	−0.03	0.00	0.49
Ga(1)−H(12A)	0.040(1)	0.466(1)	2.912	1.14	1.77	1.36	0.03	−0.02	0.01	0.64
	0.050	0.417		1.13	1.76	0.60	0.02	−0.02	0.00	0.49
Ga(1)−H(21A)	0.041(1)	0.497(1)	2.884	1.11	1.78	2.86	0.03	−0.02	0.01	0.66
	0.052	0.470		1.12	1.75	2.87	0.03	−0.02	0.00	0.54
Ga(1)−H(24C)	0.048(2)	0.598(1)	2.700	1.09	1.61	0.29	0.03	−0.02	0.01	0.69
	0.069	0.500		1.08	1.62	0.15	0.03	−0.03	0.00	0.46
					C···H−C Interactions					
C(1)−H(8)	0.102(2)	1.307(1)	2.318	1.00	1.47	3.26	0.08	−0.07	0.01	0.77
	0.103	1.324		0.96	1.37	0.65	0.08	−0.07	0.01	0.78
C(1)−H(23)	0.100(3)	1.277(2)	2.354	0.95	1.39	2.98	0.08	−0.06	0.01	0.77
	0.098	1.269		0.98	1.40	1.22	0.08	−0.06	0.01	0.77

[a] First row data from model **A**, second row from **C**.

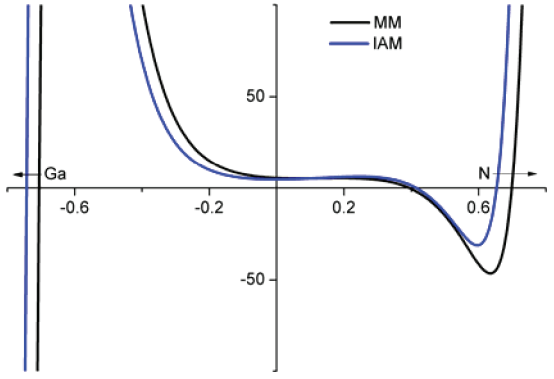

Figure 3. The Laplacian of $\rho(r)$ along the Ga−N(1) bond path. The y-axis is located at the position of the bcp in the Ga(1)−N(1) bond.

identical. Further, the differences in the ellipticities vanish in the topological analysis of the theoretical density. On the other hand, the guanidinate N−C bonds all have ε values in the range that suggests π-type character. Again, in this group of bonds, the ε values show a dispersion which is not necessarily significant, as the longer C−N(3) bond may be expected to have the lowest value of ε, contrary to the experimental model **A**.

As mentioned above, the Ga−N bonds show signs of covalency judging from the significantly negative value of the total energy density, $H(r)$, which suggests that the potential energy density, $V(r)$, dominates at the bcp. The greater $|V(r)|$ than $G(r)$ may be interpreted such that electrons have a tendency to accumulate in the bcp region. However, this impression is not conveyed by the behavior of the Laplacian along the Ga−N bond, as shown in Figure 3. Instead, this shows a positive value of the Laplacian in an extended region (±0.4 Å) around the bcp, which on the N-side goes into a valence shell charge concentration, or lone pair, while no evidence for valence shell charge concentration on Ga is visible, similar to previous observations for elements after and including the 3d metals. The shape of Figure 3 may indicate that the Ga−N interaction is more correctly termed a dative bond, with little covalent contribution: this will be examined in more detail below. In Figure 3 the curve from an IAM model is also included, showing very little difference in the bcp region.

As highlighted in Figure 1, four Ga···H−C contacts were found in both experimental and theoretical data in addition to the anticipated bonds within the covalent framework of **1**. Table 2 reports properties at the bcp's corresponding to these, showing electron density to be an order of magnitude less than in the Ga−N bonds. To investigate in more detail whether these contacts could be termed hydrogen bonds, we have applied the criteria proposed by Koch and Popelier for C−H···O hydrogen bonds[35] to these contacts, with full details reported in Supporting Information Table S6. In all four cases, the electron density and

dx.doi.org/10.1021/ic2009946 |*Inorg. Chem.* 2011, 50, 8418–8426

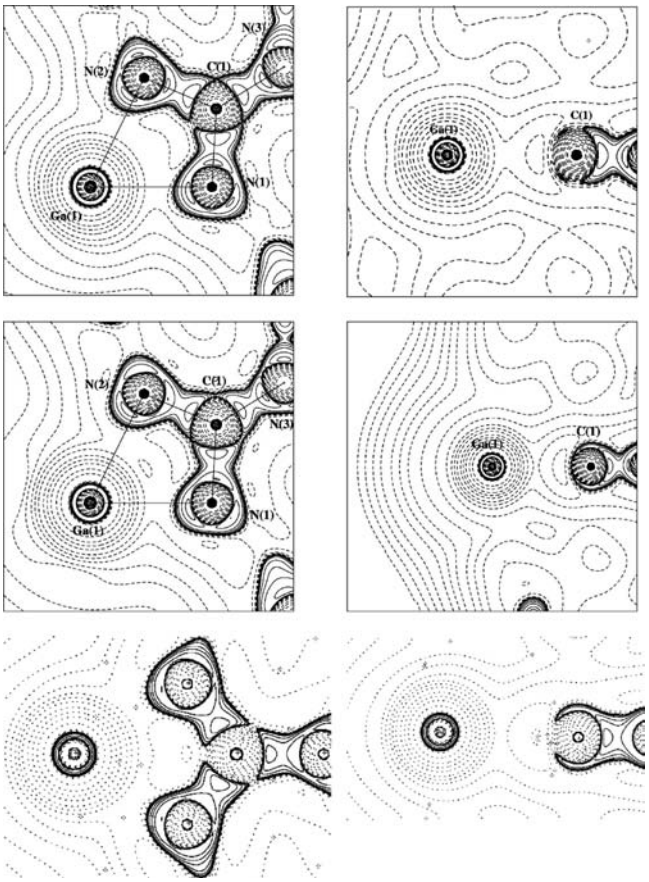

Figure 4. Two-dimensional plots of $\nabla^2\rho(r)$ showing (left) the Ga−N−C−N plane and (right) a perpendicular section through the Ga−N−C−N plane containing the Ga−C line. First line shows model **A**, second line model **B**, and the third line model **C**. Solid contours show positive values of the Laplacian, and dashed lines show negative values at intervals of 2, 4, 8 × 10^n, with n an integer between −3 and 6.

its Laplacian are within the ranges set out for hydrogen bonding. Koch and Popelier also specify changes in density and atomic properties between isolated monomers and complexes that signify hydrogen bonding: in this intramolecular case, "monomer" properties cannot be evaluated. Instead, we compare properties of the hydrogens involved in the C−H···Ga contacts with those of analogous hydrogens not involved in any contact. One of the key criteria for hydrogen bonding is mutual penetration of the atoms involved, such that bonded radii are less than nonbonded radii. We estimate the nonbonded radius of a hydrogen in an isopropyl as 0.93 Å,[36] significantly less than the bonded radii extracted from Table 2 as the distances from H to the bcp in the Ga−H interaction, such that all four contacts fail this test. Other criteria are loss of electron population, energy, dipole polarization, and volume of the hydrogen atom. All four hydrogens have smaller volumes and dipole moments than their counterparts, but only H12(A) and H21(A) fulfill the population and energy criteria. It may well be that the criteria proposed for C−H···O contacts are inappropriate for C−H···Ga ones, but the lack of mutual penetration suggests that the interactions should not be termed hydrogen bonds. A more detailed theoretical study of model systems is underway and will be reported in due course.

The coordination chemistry of **1** and related molecules is dominated by the ability of the Ga center to act as an electron pair

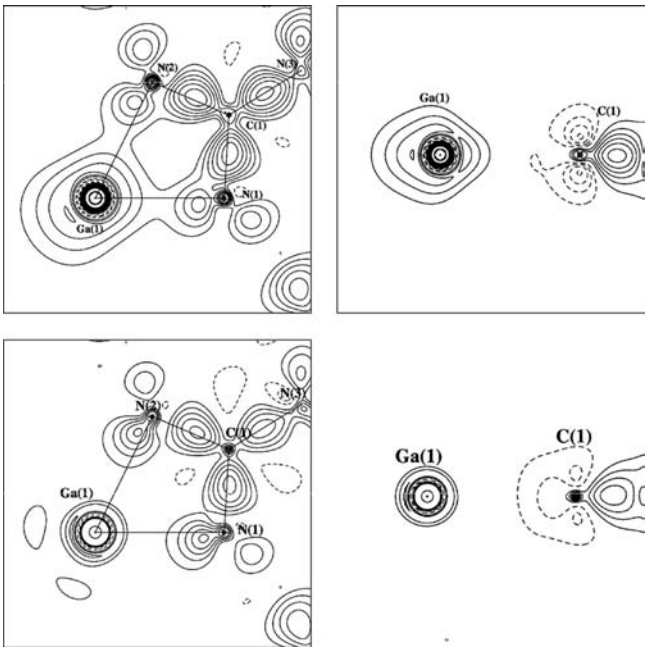

Figure 5. Static deformation density plots in the same planes as Figure 4, based on a reference model with a neutral Ga at the Ga(1) site, from model **A** (top) and **B** (bottom). The difference plots show positive density as solid lines and negative density as dashed lines at intervals of ±0.1 e $Å^{-3}$. The zero contour has been omitted.

donor. To probe this ability in more detail, plots of $\nabla^2\rho(r)$ from the final experimental model, along with equivalent theoretical data, are shown in Figure 4. These plots reveal almost complete sphericity of the density around Ga, and outside the core region of Ga the Laplacian values are uniformly positive. No feature is present that may indicate a lone pair of electrons, which is further evidenced by the failure to locate any maxima in the Laplacian in the valence shell of Ga from either experimental or theoretical data. A one-dimensional plot away from the GaNCN ring (see Figure S4, Supporting Info) shows positive $\nabla^2\rho(r)$ over the entire valence shell, albeit with a slight deviation from monotonic decrease between 1.1 and 1.4 Å. Within the four-membered ring, the covalent nature of the N−C bonds is apparent from these plots, as are the lone pairs on N(1) and N(2) directed toward Ga. Agreement between experiment and theory is again excellent in all plots considered.

It is interesting to note the slight differences near the central C(1) above and below the Ga heterocycle plane. The C(1) atom is covered by lobes of negative $\nabla^2\rho$ in models **B** and **C**, whereas no such negative lobes are present in the experimental model **A**. In both of these directions, C(1) is involved in hydrogen bonding with H(8) and H(23) from the tertiary C−H of the isopropyl groups, with distinct bcp's found. Properties evaluated at these C−H···C hydrogen bonds are also reported in Table 2, showing slightly higher electron density and Laplacian values than the C−H···Ga contacts. There is a difference of only 0.03 Å in the hydrogen bond distances (2.32 and 2.35 Å, respectively, to H(8) and H(23)). This similarity is mirrored in their topological properties, but the bond path is only entirely straight for the C(1)−H(8) bond, not so for the C(1)−H(23) interaction. While this type of hydrogen bond is unusual, a search in the CSD reveals nine structures with H···C distances below 2.35 Å between a R_3CH group and a CN_3 moiety, with the shortest

dx.doi.org/10.1021/ic2009946 |*Inorg. Chem.* 2011, 50, 8418–8426

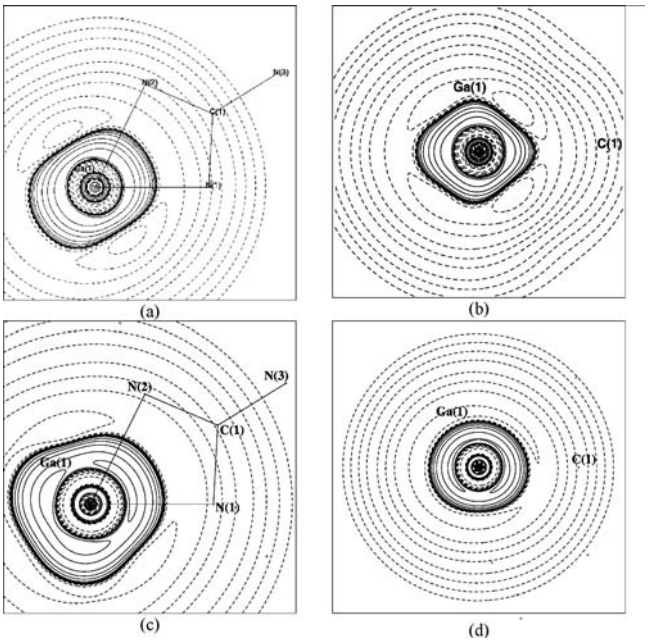

Figure 6. $\nabla^2\rho$-distributions for (left column) the Ga−N−C−N plane and (right) the perpendicular plane, as defined for Figure 4, (a) and (b) from model **A**, (c) and (d) from model **B**, using only the Ga 4s,4p valence electrons. Contours as in Figure 4.

interaction being 2.31 Å.[37] C−H···C hydrogen bonds have also been observed on the basis of theoretical data.[38]

Figure 5 shows plots analogous to Figure 4 of the static deformation density from models **A** and **B**, which indicates some preferred orientation of the density, pointing in the expected region of a lone pair of electrons. The large deviations near the nucleus of Ga may be due to the lack of core scaling in the reference model used for subtraction in the deformation density. Significant reorganization of electron density relative to neutral, spherical atoms is apparent in the valence regions of all atoms shown, with values of 0.5−0.6 e Å^{-3} accumulated in the covalent N−C bonds, while accumulation of 0.3−0.4 e Å^{-3} is evident in the Ga lone pair region. The presence of such a feature on Ga is particularly striking, because the density of a neutral atom is subtracted from the formally Ga^+ center and is in marked contrast to the spherical Laplacian plots in Figure 4. The positive deformation density in the lone pair region of Ga extends further in the experimental model **A** than in model **B**. However, it is clear that both present a maximum exactly opposite the Ga−C(1) direction in the expected lone pair region.

To analyze this feature further, plots of $\nabla^2\rho(r)$ from only the Ga valence electrons are shown in Figure 6. In models **A** and **B**, there are slightly less than three electrons in the Ga valence shells. The plots in Figure 6 are in much better agreement with the findings from the deformation density and confirm the presence of accumulation of valence density in the lone pair region of Ga compared to the regions around it. The noticeable difference between all-electron (Figure 4) and valence-only (Figure 6) plots of $\nabla^2\rho(r)$ suggests that this lone pair density, which stems from about three electrons, is "swamped" by the Ga core contributions to the extent that it becomes invisible in all-electron Laplacian plots. This also explains why, as mentioned above, it has not been possible to locate any (3,−3) critical points in the Laplacian distribution around the Ga in the total electron density, which

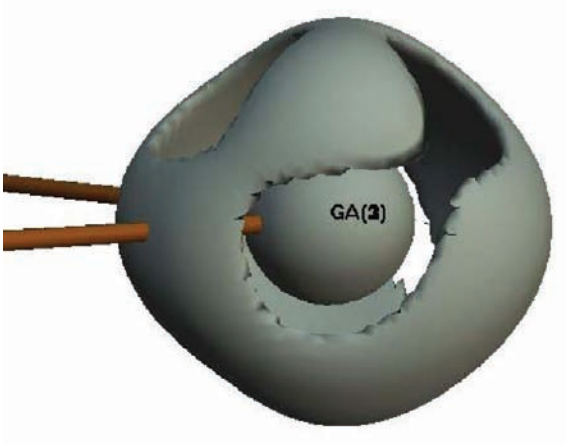

Figure 7. Three-dimensional Laplacian distribution from the valence electron density only of model **A** using the isosurface value of −10 e Å^{-5}.

would normally identify a region of charge concentration attributable to a lone pair, such as it has consistently been observed in theoretical and experimental charge density studies of N-heterocyclic compounds[5b] and cyclopropenylidenes.[39] It should be noted that we were unable to definitively separate core and valence canonical molecular orbitals, so analogous plots from model **C** could not be obtained. However, it is notable that these valence density features are found in the same region as the deviation from monotonic decrease in radial Laplacian shown in Figure S4 (Supporting Information). In this context, it is striking that if the Ga 3d-electrons are retained as valence electrons, the lone pair features on Ga disappear and the Laplacian around Ga resembles that seen in Figure 4. It is important to notice that in the expected lone pair region a (3,−1) or saddle point in the negative Laplacian is located, rather than the (3,−3) or local maximum seen in carbon compounds. Thus, the theoretical assignment of a lone pair on Ga is called into question by the experimental data. This fascinating contrast between light and heavy p-block compounds is one which we are currently investigating, with results to follow in a subsequent publication.

Directionality in the valence-only $\nabla^2\rho(r)$ distribution is shown more clearly as an isosurface representation in Figure 7. It is evident that this distribution possesses some structure beyond that seen in Figure 6, which we ascribe to ligand-induced charge concentrations (LICCs), or minima in $\nabla^2\rho(r)$, whose spatial distribution is shown in Figure S5 (Supporting Information). This analysis reveals two distinct LICCs toward both the N atoms as well as two more LICCs opposite the heterocycle, thus resembling a square planar arrangement around Ga, with valence density LICCs located approximately 0.6 Å from the Ga nucleus. Model **A** also exhibits two further LICCs inclined to the heterocycle plane, almost oriented toward the two strongest Ga···H interactions with H(9C) and H(24C), having Ga−LP−H angles close to 150°, which may suggest that these interactions are quite directional in nature.

The presence of a valence lone pair in **1** is further supported by plots of the molecular electrostatic potential (MEP) calculated from models **A** and **C**, projected onto the 0.001 au electron density isosurface, as shown in Figure 8. A large area of negative MEP (minimum = −22.4 kcal mol^{-1} in **C**) is present in the expected lone pair region of Ga, along with shallower minima associated with the aromatic rings. The ability of the isopropyl

dx.doi.org/10.1021/ic2009946 |*Inorg. Chem.* 2011, 50, 8418–8426

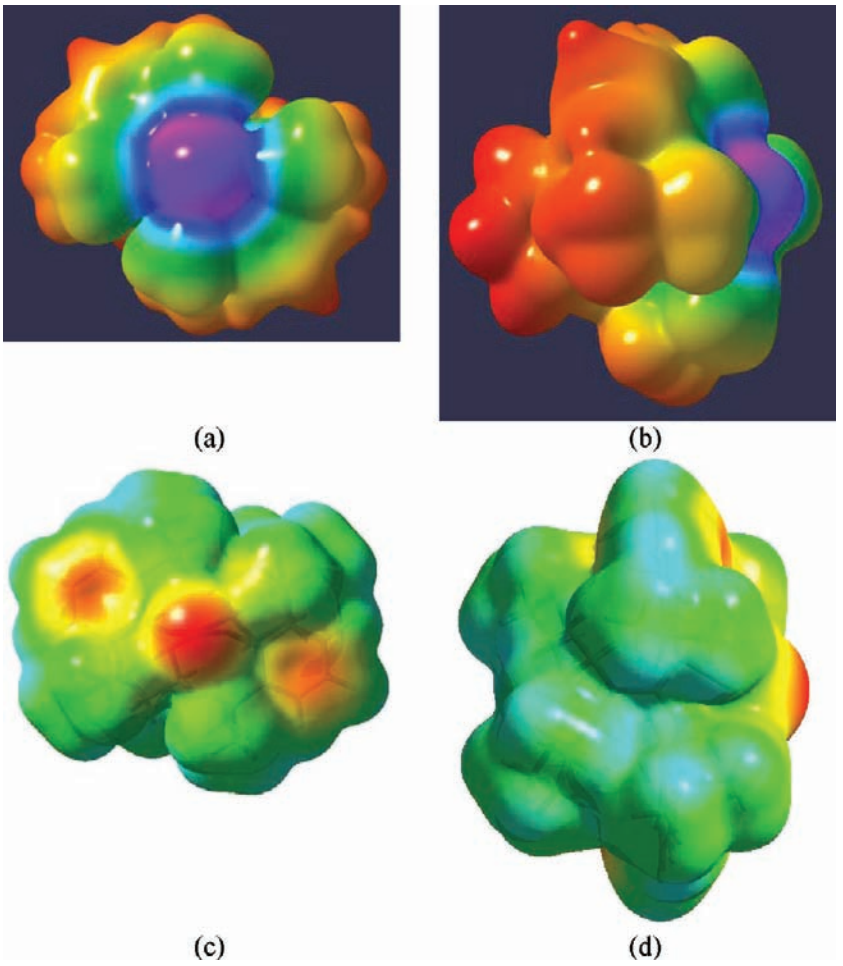

Figure 8. Electrostatic potential mapped onto 0.001 au density surface, shown from two perpendicular directions. First row is from experimental data model **A** and second row is from theoretical data model **C**. The orientation is such that in (a) and (c) the view is along the Ga···C line in the heterocycle, while (b) and (d) show the molecule side-on parallel to the heterocycle, and Ga to the right.

groups to protect the Ga center but leave enough of the surface of this atom exposed to react is also apparent from these plots.

As well as local properties of the electron density, evaluation of integrated properties over atomic basins gives complementary information on the electron distribution in **1**. Results for selected atoms are reported in Table 3. This procedure proceeded smoothly for the N and C atoms reported, but the split-core scaling of the Ga core meant that the normal integration procedure, using the TOPXD module of XD,[40] failed for Ga, leading to a deviation from overall charge neutrality of the molecule.[41] Table 3 therefore also reports atomic charges and volumes, calculated over atomic basins directly from a three-dimensional grid of total electron density using the BADER program.[42] Satisfactory integration was ensured by checking that the sum of atomic populations was within 0.005 e of the total number of electrons in the molecule.

Our best estimate of the atomic charge of Ga from model **A** is +0.19, as obtained from the grid-based method. In light of the problems noted above, this is a more reliable estimate of atomic charge than the +0.04 obtained from TOPXD. Rather larger positive charges are obtained from theoretical data, support for which comes from NBO analysis, which gives a charge of +0.71 on Ga, very similar to that previously reported for a model compound.[8] Evidence for the oxidation state of Ga is therefore rather mixed, although all data except the suspect TOPXD values agree that Ga carries a partial positive charge with a numerical value of rather less than +1. Charges on N and C atoms are in

Table 3. Integrated Atomic Properties (au)[a]

	Q_{AIM} (vol_{AIM})	Q_{BADER}	L_{AIM}	μ_{AIM}	loc (%)
Ga(1)	+0.044(182.46)	+0.188(202.3)	5.01×10^{-4}	1.021	
	+0.618(217.57)	+0.629(245.7)	-9.32×10^{-5}	1.711	97.4
N(1)	−1.141(78.9)	−1.147(78.2)	2.90×10^{-3}	0.195	
	−1.244(82.6)	−1.240(79.3)	1.33×10^{-4}	0.223	78.3
N(2)	−1.151(79.5)	−1.134(74.8)	1.59×10^{-3}	0.218	
	−1.243(82.0)	−1.251(78.4)	-1.20×10^{-4}	0.219	78.3
N(3)	−1.159(69.2)	−1.146(66.2)	3.55×10^{-3}	0.059	
	−1.072(67.9)	−1.075(66.5)	1.81×10^{-4}	0.127	76.6
C(1)	+1.121(33.5)	+1.135(33.6)	2.10×10^{-4}	0.008	
	+1.425(31.3)	+1.429(34.2)	6.36×10^{-4}	0.066	60.7

[a] First line gives model **A**, second line model **C**. The values for L and μ correspond to AIM integrations, while localization in the final column comes only from DFT data. Volumes are given in parentheses next to the atomic charges. L should be zero for satisfactory integration over an atomic basin and so gives an estimate of the accuracy of numerical integration.

dx.doi.org/10.1021/ic2009946 |*Inorg. Chem.* 2011, 50, 8418–8426

better agreement between methods, both showing negatively charged nitrogens and positively charged C(1), as might be expected on electronegativity grounds. Unlike the case of Ga, methods of calculating atomic charges are consistent with one another within each model, although differences of ca. 0.1 e are apparent in charges on N and 0.3 e in C(1).

Both experiment and theory show significant dipolar polarization of Ga, the sign of which indicates that the centroid of density within Ga's basin is shifted toward the lone pair region, thus supporting the conclusions drawn from maps above. Similarly, a large negative eigenvalue of the quadrupole moment tensor on Ga indicates that density is concentrated into the lone pair region and depleted in orthogonal directions. The volume of the Ga basin, truncated by interatomic surfaces and the 0.001 au density surface, is very large at more than twice the values for N. As is commonly the case, the DFT value is significantly larger than the multipole-derived one, because the former is taken from an isolated gas-phase molecule with no intermolecular contacts, whereas the latter is an in-crystal value.

Integration of the overlap matrix over atomic basins defined from model **C** allows calculation of the atomic overlap matrix (AOM), from which localization and delocalization indices may be derived. The localization of the electron density in a region Ω is determined by the fraction of the total Fermi correlation contained within the boundaries of that region, the maximum value of the Fermi correlation being $-N(\Omega)$.[43] Such analysis is only available on theoretical data because the multipole model used for experimental data does not contain the necessary orbital overlap matrix. Table 3 reports localization within the atomic basins of selected atoms and shows that the density within the basin of Ga(1) is highly localized. Of course, the localization of Ga(1) is strongly affected by its large core: if 18 electrons corresponding to the [Ar] core are omitted from this analysis a value of 93.7% is obtained, still very high. Omitting a further 10 3d electrons results in a value of 67.3%, indicating that the 4s and 4p electrons are significantly delocalized. In contrast, nitrogens and especially C(1) are highly delocalized, a result which is expected given the delocalized nature of the Giso ligand. The AOM can also be used to derive bond orders from the extent to which the Fermi correlation extends across interatomic surfaces.[44] In this case, we calculate Ga−N bond orders of 0.49 for both bonds, in good agreement with the conclusions drawn from the energy density at the bond critical point in Table 2. It seems, therefore, that the Laplacian of the electron density is less useful than energy density as a descriptor of covalent bonding, as is often the case for heavier elements.[45] Bond orders of 1.10 for both N−C bonds within the ring and of 1.04 for N(3)−C(1) are commensurate with the delocalized nature of the guanidinate ligand.

CONCLUSIONS

This study has highlighted the utility of experimental charge density analysis for the study of the unusual bonding and electronic properties of low oxidation state p-block systems. The observation that not only the valence density but also the core density of Ga^+ bound in a molecule are significantly different from the density of the free Ga atom or Ga^+ ion is remarkable. The fact that the experimental and theoretical data show strikingly similar extents of radial contraction of the 3d-shell and coexistent expansion of the s,p-electrons suggests that this is a real physical effect due to the onset of chemical bonding.

Once a suitable model for the scattering from Ga is obtained, investigation of the valence electron density distribution from experimental data becomes possible. The chemistry of **1** is dominated by its ability to act as a relatively strong σ-donor but weak π-acceptor, properties which are rationalized on the basis of the observed electron density. Unambiguous evidence for the presence of lone pair density on Ga is found from static deformation density plots, but similar features are only present in Laplacian plots once the swamping effect of the 3d-electrons is removed. The lone pair, predicted by DFT calculations to have primarily s-character, shows significant directionality that leads it to point away from the heterocycle. This is also evident in the molecular electrostatic potential that, when plotted in on a rendering of the molecular surface, manifests itself as a large electronegative region, ready to interact with metal ions. However, despite the chemical analogy between **1** and N-heterocylic carbenes, the lone pair density shows a significant difference between Ga and C centers, with the lone pair in **1** corresponding to a saddle point rather than a local minimum in the Laplacian of the density. The weak π-acceptor ability of **1** is evident from the lack of overlap between formally filled π-type nitrogen lone pairs and the empty p-orbital on Ga, leading to purely σ-character in Ga−N bonding . In summary, we believe that such analyses will prove useful as an experimental "yardstick" by which to measure the reliability of the many theoretical techniques that have been applied to the study of low oxidation state main group complexes.

ASSOCIATED CONTENT

Supporting Information. Detailed description of data collection, reduction and refinement, further justification and analysis of split-core scaling model, comparison of multipole parameters between models **A** and **B**, full topological analysis of model **A**, details of Ga−H "hydrogen bond" criteria, spatial location of minima in $\nabla^2\rho(r)$ distribution, and crystal data. This material is available free of charge via the Internet at http://pubs.acs.org.

AUTHOR INFORMATION

Corresponding Author
*E-mail: jacobo@chem.au.dk.

ACKNOWLEDGMENT

The Danish Research Council is gratefully acknowledged for supporting a collaborative visit to Monash University for J.O. The Australian Research Council is acknowledged (fellowship for C.J. and Discovery Project Grant DP0665057).

REFERENCES

(1) For representative reviews since 2007, see: (a) Fischer, R. C.; Power, P. P. *Chem. Rev.* **2010**, *110*, 3877–3923. (b) Schulz, S. *Chem.—Eur. J.* **2010**, *16*, 6416–6428. (c) Krieck, S.; Yu, L.; Reiher, M.; Westerhausen, M. *Eur. J. Inorg. Chem.* **2010**, No. 2, 197–216. (d) Wang, Y. Z.; Robinson, G. H. *Chem. Commun.* **2009**, 5201–5213. (e) Mizuhata, Y.; Sasamori, T.; Tokitoh, N. *Chem. Rev.* **2009**, *109*, 3479–3511. (f) Nagendran, S.; Roesky, H. W. *Organometallics* **2008**, *27*, 457–492. (g) Rivard, E.; Power, P. P. *Inorg. Chem.* **2007**, *46*, 10047–10064. (h) Power, P. P. *Organometallics* **2007**, *26*, 4362–4372. (i) Schnöckel, H. *Dalton Trans.* **2007**, 4344. (j) Wang, Y. Z.; Robinson, G. H. *Organometallics* **2007**, *26*, 2–11. (k) Pardoe, J. A. J.; Downs, A. J. *Chem. Rev.* **2007**, *107*, 2.

(2) See for example: (a) Zhu, Z. L.; Fischer, R. C.; Ellis, B. D.; Rivard, E.; Merrill, W. A.; Olmstead, M. M.; Power, P. P.; Guo, J. D.; Nagase, S.; Pu, L. H. *Chem.—Eur. J.* **2009**, *15*, 5263–5272. (b) Peng, Y.; Fischer, R. C.; Merrill, W. A.; Fischer, J.; Pu, L. H.; Ellis, B. D.; Fettinger, J. C.; Herber, R. H.; Power, P. P. *Chem. Sci.* **2010**, *1*, 461–468.

(3) (a) Su, J. R.; Li, X. W.; Crittendon, R. C.; Campana, C. F.; Robinson, G. H. *Organometallics* **1997**, *16*, 4511–4513. (b) Cotton, F. A.; Feng, X. J. *Organometallics* **1998**, *17*, 128–130. (c) Robinson, G. H. *Acc. Chem. Res.* **1999**, *32*, 773–782. (d) Hardman, N. J.; Wright, R. J.; Phillips, A. D.; Power, P. P. *J. Am. Chem. Soc.* **2003**, *125*, 2667–2679.

(4) Bader, R. F. W. *Atoms in Molecules: A Quantum Theory*; Clarendon Press: Oxford, U.K., 1990.

(5) (a) Koritsanszky, T. S.; Coppens, P. *Chem. Rev.* **2001**, *101*, 1583–1627. (b) Tafipolsky, M.; Scherer, W.; Öfele, K.; Artus, G.; Pedersen, B.; Herrmann, W. A.; McGrady, G. S. *J. Am. Chem. Soc.* **2002**, *124*, 5865–5880. (c) Whitten, A. E.; Dittrich, B.; Spackman, M. A.; Turner, P.; Brown, T. C. *Dalton Trans.* **2004**, 23–29.

(6) Jana, A.; Leusser, D.; Objartel, I.; Roesky, H. W.; Stalke, D. *Dalton Trans.* **2011**, *40*, 5458–5463.

(7) (a) Overgaard, J.; Jones, C.; Stasch, A.; Iversen, B. B. *J. Am. Chem. Soc.* **2009**, *131*, 4208–4209. (b) Platts, J. A.; Overgaard, J.; Jones, C.; Iversen, B. B.; Stasch, A. *J. Phys. Chem. A* **2011**, *115*, 194–200.

(8) Jones, C.; Junk, P. C.; Platts, J. A.; Stasch, A. *J. Am. Chem. Soc.* **2006**, *128*, 2206–2207.

(9) Jones, C. *Coord. Chem. Rev.* **2010**, *254*, 1273–1289.

(10) Asay, M.; Jones, C.; Driess, M. *Chem. Rev.* **2011**, *111*, 354–396.

(11) (a) Moxey, G. J.; Jones, C.; Stasch, A.; Junk, P. C.; Deacon, G. B.; Woodul, W. D.; Drago, P. R. *Dalton Trans.* **2009**, 2630–2636. (b) Jones, C.; Stasch, A.; Moxey, G. J.; Junk, P. C.; Deacon, G. B. *Eur. J. Inorg. Chem.* **2009**, 3593–3599. (c) Green, S. P.; Jones, C.; Stasch, A. *Inorg. Chem.* **2007**, *46*, 11–13.

(12) Flierler, U.; Burzler, M.; Leusser, D.; Henn, J.; Ott, H.; Braunschweig, H.; Stalke, D. *Angew. Chem., Int. Ed.* **2008**, *47*, 4321–4325.

(13) Bader, R. F. W.; Essen, H. *J. Chem. Phys.* **1984**, *80*, 1943–1960.

(14) Scherer, W.; Sirsch, P.; Shorokhov, D.; Tafipolsky, M.; McGrady, G. S.; Gullo, E. *Chem.—Eur. J.* **2003**, *9*, 6057–6070.

(15) McGrady, G. S.; Haaland, A.; Verne, H. P.; Volden, H. V.; Downs, A. J.; Shorokhov, D.; Eickerling, G.; Scherer, W. *Chem.—Eur. J.* **2005**, *11*, 4921–4934. Scherer, W.; Herz, V.; Brück, A.; Hauf, C.; Reiner, F.; Altmannshofer, S.; Leusser, D.; Stalke, D. *Angew. Chem., Int. Ed.* **2011**, *50*, 2845–2849. Scherer, W.; Hauf, C.; Presnitz, M.; Scheidt, E.-W.; Eickerling, G.; Eyert, V.; Hoffmann, R.-D.; Rodewald, U. C.; Hammerschmidt, A.; Vogt, C.; Röttgen, R. *Angew. Chem., Int. Ed.* **2010**, *49*, 1578–1582, and references therein.

(16) *CrysAlisPro*, Version 1.171.34.36; Oxford Diffraction Ltd.: Oxford, U.K., 2010.

(17) *CrysAlisPro*, Version 1.171.34.49; Agilent Technologies: Oxford, U.K., 2010. Program ABSPACK for numerical absorption correction based on gaussian integration over a multifaceted crystal model.

(18) Blessing, R. H. *J. Appl. Crystallogr.* **1997**, *30*, 421–426.

(19) Sheldrick, G. M. *Acta Crystallogr., Sect. A: Found. Crystallogr.* **2008**, *64*, 112–122.

(20) Hansen, N. K.; Coppens, P. *Acta Crystallogr., Sect. A: Cryst. Phys., Diffr., Theor. Gen. Crystallogr.* **1979**, *39*, 909–921.

(21) Volkov, A.; Macchi, P.; Farrugia, L. J.; Gatti, C.; Mallinson, P.; Richter, T.; Koritsanszky, T. *XD2006*; State University of New York at Buffalo: Buffalo, NY, 2006. A computer program package for multipole refinement, topological analysis of charge densities and evaluation of intermolecular energies from experimental and theoretical structure factors.

(22) Madsen, A. Ø.; Sørensen, H. O.; Flensburg, C.; Stewart, R. F.; Larsen, S. *Acta Crystallogr., Sect. A: Found. Crystallogr.* **2004**, *60*, 550–561.

(23) Overgaard, J.; Iversen, B. B. *Struct. Bonding (Berlin, Ger.)* **2011**No. 10.1007/430_2010_28, in press.

(24) Hoser, A. A.; Dominiak, P. M.; Wozniak, K. *Acta Crystallogr., Sect. A: Found. Crystallogr.* **2009**, *65*, 300–311.

(25) Allen, F. H.; Kennard, O.; Watson, D. G.; Brammer, L.; Orpen, A. G.; Taylor, R. J. *J. Chem. Soc., Perkin Trans. 2* **1987**, 1–19.

(26) (a) Munshi, P.; Madsen, A. O.; Spackman, M. A.; Larsen, S.; Destro, R. *Acta Crystallogr., Sect. A: Found. Crystallogr.* **2008**, *64*, 465–475. (b) Madsen, A. O. *J. Appl. Crystallogr.* **2006**, *39*, 757–758.

(27) (a) Becke, A. D. *Phys. Rev. A: At., Mol., Opt. Phys.* **1988**, *38*, 3098–3100. (b) Perdew, J. P. *Phys. Rev. B: Condens. Matter Mater. Phys.* **1986**, *33*, 8822–8824. (c) Hehre, W. J.; Ditchfie., R; Pople, J. A. *J. Chem. Phys.* **1972**, *56*, 2257. (d) Francl, M. M.; Pietro, W. J.; Hehre, W. J.; Binkley, J. S.; Gordon, M. S.; Defrees, D. J.; Pople, J. A. *J. Chem. Phys.* **1982**, *77*, 3654–3665. (e) Clark, T.; Chandrasekhar, J.; Spitznagel, G. W.; Schleyer, P. V. *J. Comput. Chem.* **1983**, *4* (3), 294–301.

(28) Frisch, M. J. et al. *Gaussian 03*, Revision C.02; Gaussian, Inc.: Wallingford CT, 2004.

(29) (a) Biegler-König, F. W.; Bader, R. F. W.; Tang, T. H. *J. Comput. Chem.* **1982**, *3*, 317–328. (b) Biegler-König, F.; Schonbohm, J. *J. Comput. Chem.* **2002**, *23*, 1489–1494.(c) Keith, T. A. *AIMAll*; 2009. Available from http://aim.tkgristmill.com.

(30) Reed, A. E.; Weinstock, R. B.; Weinhold, F. *J. Chem. Phys.* **1985**, *83*, 735–746.

(31) Volkov, A.; Koritsanszky, T.; Chodkiewicz, M.; King, H. F. *J. Comput. Chem.* **2009**, *30*, 1379–1391.

(32) Volkov, A.; Macchi, P. VM data bank in XD. Unpublished results.

(33) Zhurov, V. V.; Zhurova, E. A.; Stash, A. I.; Pinkerton, A. A. *Acta Crystallogr., Sect. A: Found. Crystallogr.* **2011**, *67*, 160–173.

(34) Pillet, S.; Souhassou, M.; Lecomte, C.; Schwarz, K.; Blaha, P.; Rerat, M.; Lichanot, A.; Roversi, P. *Acta Crystallogr., Sect. A: Found. Crystallogr.* **2001**, *57*, 290–303.

(35) Koch, U.; Popelier, P. L. A. *J. Phys. Chem.* **1995**, *99*, 9747–9754.

(36) Nonbonded radius was estimated as the distance to the 0.001 au density surface along the C−H direction, averaged over eight isopropyl hydrogens not involved in any intramolecular contact. Atomic properties of "typical" isopropyl hydrogens were averaged over the same eight atoms.

(37) Green, S. P.; Jones, C.; Stasch, A. *Inorg. Chem.* **2007**, *46*, 11–13.

(38) (a) Platts, J. A.; Howard, S. T.; Wozniak, K. *Chem. Commun.* **1996**, 63–64. (b) Platts, J. A.; Howard, S. T. *J. Chem. Soc., Perkin Trans. 2* **1997**, 2241–2248.

(39) Scherer, W.; Tafipolsky, M.; Öfele, K. *Inorg. Chim. Acta* **2008**, *361*, 513–520.

(40) Volkov, A.; Gatti, C.; Abramov, Y.; Coppens, P. *Acta Crystallogr., Sect. A: Found. Crystallogr.* **2000**, *56*, 252–258.

(41) In practice, three atoms were placed on the Ga site with separate zero-flux surfaces. If TOPXD was able to find the zero-flux surface resulting from the three densities, then separate integrations of the three densities within the same surface would give the correct result. However, that does not happen, and we speculate that the program is not able to treat the three atomic densities as one when defining the zero-flux surface. Instead, it is likely that somehow the valence electrons are counted twice, which would also give an atomic charge around +0.6.

(42) Henkelman, G.; Arnaldsson, A.; Jonsson, H. *Comput. Mater. Sci.* **2006**, *36*, 354–360.

(43) Bader, R. F. W.; Stephens, M. E. *J. Am. Chem. Soc.* **1975**, *97*, 7391–7399.

(44) Angyan, J. G.; Loos, M.; Mayer, I. *J. Phys. Chem.* **1994**, *98*, 5244–5248.

(45) Gatti, C.; Lasi, D. *Faraday Discuss.* **2007**, *135*, 55–78.